IEICE TRANS. COMMUN., VOL.E84–B, NO.3 MARCH 2001

PAPER

# A Ray-Tracing-Based Characterization and Verification of the Spatio-Temporal Channel Model for Future Wideband Wireless Systems

**Houtao ZHU**[†], ***Student Member***, **Jun-ichi TAKADA**[††], **Kiyomichi ARAKI**[††], ***and*** **Takehiko KOBAYASHI**[†††], ***Regular Members***

**SUMMARY** A proper design and analysis of future wideband wireless communication systems require an accurate radio channel model. This model is claimed to characterize both the spatial and temporal channel characteristics. This paper investigates the spatio-temporal channel modeling based on a ray-tracing approach. The temporal channels are characterized by a delay profile. The statistical median and fading-fluctuation range of delay profiles are predicted from ray tracing by incorporating the random phase approach. A high level of agreement between predicted results and measured ones is observed in the verification. The spatio-temporal channel impulse response (CIR) predicted from ray tracing is also transformed to have limited bandwidth and limited beam-width characteristics. The applicability of this transformation is also verified by the comparison with measurement. These verifications prepare the ground for the use of ray-tracing approaches to evaluate system performance in real environments.

***key words:*** *channel modeling, spatio-temporal channel model, ray-tracing, random-phase approach*

## 1. Introduction

It is well known that the multipath and time-varying nature of wireless propagation channels incurs the fundamental problems for wireless systems. For narrowband systems, these characteristics cause the problems of signal level fluctuation (multipath fading) and Doppler shifts of received signals. For wideband systems, besides these problems, time-dispersion effects of the channels are of great concerns. Recent researches [1] on future wireless systems (e.g., third and fourth generation mobile systems) have discovered the necessity of exploring the spatial properties of the wireless channels. For example, smart antennas utilize the spatial filtering technique to improve the received signal quality by spatially separating the users. Therefore, the prerequisite for the proper design and analysis of these systems is an accurate channel model that incorporates the spatial and temporal characteristics of wireless channels [2].

Many spatial channel models [3], [4] have been proposed for this purpose. Most of these models explore the spatial distribution of the mobile stations to capture the angle of arrival (AOA) characteristics of the channel. These models are in nature statistical channel models, which are appropriate for the evaluation of channel transmission characteristics in a general sense. They may not be very suitable for the evaluation of system performance in real environments. Alternatively, with incorporating site-specific information, ray-tracing approaches [5], [6] can deterministically predict the detailed channel parameters, such as the complex channel impulse response. In this sense, ray-tracing approaches may be appropriate deterministic modeling approaches for evaluating system performance in real environments. Nevertheless, in a conventional ray-tracing simulation, there are several shortcomings as follows:

1. The received rays have the unlimited bandwidth and infinitesimally narrow beam-width. These characteristics are contrary to the real specific systems, w here the signal bandwidth is limited and the antennas have finite beam-widths. A transformation from rays (impulse) to realistic signals is necessary for the purpose of system performance evaluation. This transformation also has to be confirmed with measurement. Although [5], [6] compared the bandlimited delay profiles predicted from ray-tracing with measurement and [7] confirmed the prediction accuracy of angle-of-arrivals by ray tracing, almost no literature has reported in terms of the verification of spatial-temporal channel responses.
2. To estimate the statistics of delay profiles in a local area, the process of calculating delay profiles has to be repeated at many locations with a proper spatial sampling separation in this area. This sampling is very time-consuming since delay profiles at many receiving locations have to be estimated.

Therefore, this paper first presents a necessary

Manuscript received May 22, 2000.
Manuscript revised September 4, 2000.

[†]The author is with the Interdisciplinary Graduate School of Science and Engineering, Tokyo Institute of Technology, Tokyo, 152-8550 Japan.
[††]The authors are with the Graduate School of Science and Engineering, Tokyo Institute of Technology, Tokyo, 152-8552 Japan.
[†††]The author is with the YRP Mobile Telecommunications Key Technology Research Laboratories Co., Ltd, Yokosuka-shi, 239-0847 Japan.

transformation from rays (impulse) to realistic signals for the purpose of system performance evaluation. A spatio-temporal channel impulse response is predicted by a two dimensional-three dimensional (2D-3D) hybrid ray-tracing method [8]. An azimuth-delay profile is transformed from the CIR and then confirmed with measurement results. Second, to efficiently estimate the statistics of the local fading fluctuation, a random phase approach (RPA) [9], [10] is extended here to achieve efficiency without sacrificing accuracy at the same time. By using the RPA, only the impulse response of one receiving point is necessarily predicted from ray-tracing. The statistical median and fading-fluctuation range of delay profiles are then derived analytically. The statistics of delay profiles obtained from measurement is compared with the calculation results from RPA. The observed high-level agreement confirmed this accurate and efficient approach.

## 2. Spatio-Temporal Channel Model

In this paper the spatio-temporal channel model takes the form of a dyadic baseband complex impulse response as [8]:

$$\begin{aligned}\overline{\boldsymbol{H}}&(t,\tau,\theta^T,\phi^T,\theta^R,\phi^R)\\ &=\sum_{i=1}^{n}\begin{bmatrix}\hat{\boldsymbol{\theta}}_i^T & \hat{\boldsymbol{\phi}}_i^T\end{bmatrix}\begin{bmatrix}A_i^{\theta\theta} & A_i^{\theta\phi}\\ A_i^{\phi\theta} & A_i^{\phi\phi}\end{bmatrix}\begin{bmatrix}\hat{\boldsymbol{\theta}}_i^R\\ \hat{\boldsymbol{\phi}}_i^R\end{bmatrix}\\ &\quad\cdot\delta(\theta^T-\theta_i^T)\delta(\phi^T-\phi_i^T)\cdot\delta(\theta^R-\theta_i^R)\\ &\quad\cdot\delta(\phi^R-\phi_i^R)\cdot\delta(\tau-\tau_i)\cdot e^{j\psi_i}\cdot e^{-j\boldsymbol{k}_i\cdot\boldsymbol{v}t}\end{aligned}\quad(1)$$

where all the parameters are described as follows:

$A_i^{\theta\theta}, A_i^{\theta\phi}, A_i^{\phi\theta}, A_i^{\phi\phi}$: path gain ($A_i^{\theta\phi}$ and $A_i^{\phi\theta}$ represent cross-polarization parts)
$\hat{\boldsymbol{\theta}}_i^T, \hat{\boldsymbol{\theta}}_i^R$: unit directional vectors of vertical polarization (T: transmitter, R: receiver)
$\hat{\boldsymbol{\phi}}_i^T, \hat{\boldsymbol{\phi}}_i^R$: unit directional vectors of horizontal polarization
$\theta_i^T, \theta_i^R$: elevation angles (as seen in Fig. 1)
$\phi_i^T, \phi_i^R$: azimuth angles
$\tau_i$: delay time
$\psi_i$: phase
$\boldsymbol{k}_i$: propagation vector ($\boldsymbol{k}_i = k_0(\hat{\boldsymbol{x}}\cos\phi_i^R\sin\theta_i^R + \hat{\boldsymbol{y}}\sin\phi_i^R\sin\theta_i^R + \hat{\boldsymbol{z}}\cos\theta_i^R)$, $k_0$ is a free space wave number)
$\boldsymbol{k_i}\cdot\boldsymbol{v}t$: Doppler phase shift
$n$: total number of arrival multipath waves

This model does not include the effects of antenna structure. When the complex vector directivity patterns of transmitter and receiver antennas are expressed as

$$\boldsymbol{G}^\star(\theta^\star,\phi^\star)=G_\theta^\star(\theta^\star,\phi^\star)\hat{\boldsymbol{\theta}}^\star+G_\phi^\star(\theta^\star,\phi^\star)\hat{\boldsymbol{\phi}}^\star\quad(2)$$
$$(\star: T/R)$$

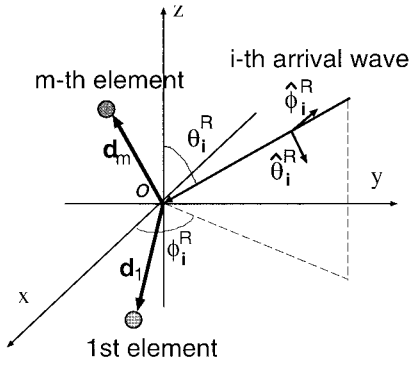


**Fig. 1** Illustration of the parameters used in the spatio-temporal channel model.

The channel impulse response $H(t,\tau)$ is expressed as:

$$\begin{aligned}H(t,\tau)=&\int_0^{2\pi}\int_0^{\pi}\int_0^{2\pi}\int_0^{\pi}\boldsymbol{G}^T(\theta^T,\phi^T)\cdot\overline{\boldsymbol{H}}\\ &\cdot\boldsymbol{G}^R(\theta^R,\phi^R)\sin\theta^T\sin\theta^R d\theta^T d\phi^T d\theta^R d\phi^R\end{aligned}\quad(3)$$

This model does neither adopt the form of the vector spatial channel impulse response (VCIR) [11], which relates the channel response at each antenna element of the array. It is easy to extend this proposed model to the form of VCIR by rotating the phase of each ray at each element. Assuming that an antenna array is employed for the receiver antenna, this extension can be expressed as follows:

$$\begin{aligned}\overline{\overline{\boldsymbol{H}}}&(t,\tau,\theta^T,\phi^T,\theta^R,\phi^R)\\ &=\begin{bmatrix}\overline{\boldsymbol{H}}_1(t,\tau,\theta^T,\phi^T,\theta^R,\phi^R)\\ \overline{\boldsymbol{H}}_2(t,\tau,\theta^T,\phi^T,\theta^R,\phi^R)\\ \vdots\\ \overline{\boldsymbol{H}}_M(t,\tau,\theta^T,\phi^T,\theta^R,\phi^R)\end{bmatrix}\end{aligned}\quad(4)$$

where

$$\begin{aligned}\overline{\boldsymbol{H}}_m&(t,\tau,\theta^T,\phi^T,\theta^R,\phi^R)\\ &=\sum_{i=1}^{n}\begin{bmatrix}\hat{\boldsymbol{\theta}}_i^T & \hat{\boldsymbol{\phi}}_i^T\end{bmatrix}\begin{bmatrix}A_i^{\theta\theta} & A_i^{\theta\phi}\\ A_i^{\phi\theta} & A_i^{\phi\phi}\end{bmatrix}\begin{bmatrix}\hat{\boldsymbol{\theta}}_i^R\\ \hat{\boldsymbol{\phi}}_i^R\end{bmatrix}\\ &\quad\cdot\delta(\theta^T-\theta_i^T)\delta(\phi^T-\phi_i^T)\cdot\delta(\theta^R-\theta_i^R)\\ &\quad\cdot\delta(\phi^R-\phi_i^R)\cdot\delta(\tau-\tau_i)\cdot e^{j\psi_i}\cdot e^{-j\boldsymbol{k}_i\cdot\boldsymbol{v}t}\\ &\quad\cdot e^{-j\boldsymbol{k}_i\cdot\boldsymbol{d_m}}\end{aligned}\quad(5)$$

where

$\boldsymbol{d_m}$: displacement vector pointing from the reference point to the $m$-th element of the array
$M$: maximum number of elements of the array

This phase-rotation ($\boldsymbol{k}_i\cdot\boldsymbol{d_m}$) is caused by the propagation of rays along the array. In fact, the given VCIR model (Eq. (4)) can be also extended to a multiple-input-multiple-output (MIMO) model by assuming an

antenna array employed at the transmitting side. In this paper, polarization and Doppler shift of the channel are not considered. They will be studied in the future.

## 3. 2D-3D Hybrid Ray-Tracing Method

The purpose of this 2D-3D hybrid ray-tracing method is the prediction of spatio-temporal channel parameters in micro- and pico-cellular environments. It launches the rays within a 2D horizontal plane with equal angle separation. The location of the reflection and diffraction points are determined by Snell's law of reflection and Keller's law of diffraction. Since all intersection points can be virtually unfolded into one plane, the heights of intersection points are determined by simple geometrical calculation and then the ray path can be established in 3D space. To decrease the computational time, a series of ray-tracing acceleration techniques are used in the ray-tracing tool, such as back-face culling, volume bounding and partition vector [10], [12]. In the field calculation, the modified Fresnel reflection coefficient for rough surface [13] and the dielectric wedge diffraction coefficient by uniform theory of diffraction [14] are used. The effect of polarization-rotation in reflection and diffraction is addressed to avoid polarization mismatch in field calculation. Since building walls may not be smooth, the roughness of reflecting surfaces is specified by the standard deviation of the surface height with respect to the mean surface height. The randomness of the surface height is assumed to be modeled by a Gaussian distribution. The authors' ray-tracing tool allows the user to specify the positions of the transmitter and the receiver, the electrical parameters (conductivity and permittivity) of every building and ground plane, carrier frequency, and the vector field directivity of antennas.

## 4. Wideband Analysis of Spatio-Temporal Channel Parameters from Ray Tracing

### 4.1 Characterization of a Delay Profile

A delay profile is a typical characteristic of temporal channel models. The impulse response predicted from ray tracing is expressed as follows:

$$h(\tau) = \sum_{l=1}^{L} A_l e^{j\psi_l} \delta(\tau - \tau_l) \tag{6}$$

where $L$ is the maximum number of arrival multipath waves. In fact, since the bandwidth of a specific system is limited, the signals arriving within a certain time period cannot be resolved. The band-limited delay profile is a result of the convolution between the impulse response and the band-limited transmission signal $P(t)$, addressed as follows:

$$\underline{h}(\tau) = \sum_{l=1}^{L} A_l e^{j\psi_l} P(\tau - \tau_l) \tag{7}$$

If the real measuring system is considered, $P(t)$ is the convolution result of the autocorrelation of the PN-sequence with the raised cosine filter. The autocorrelation of the PN-sequence is expressed as:

$$PN(t) = \begin{cases} (2^m - 1) - \dfrac{2^m}{T_b}|t| & -T_b \le t \le T_b, \\ -1 & \text{elsewhere,} \end{cases} \tag{8}$$

where

$T_b$: chip duration
$m$: stage of a shift register to generate the PN-sequence

and the impulse response of a raised-cosine filter $F(t)$ is expressed as:

$$F(t) = \mathrm{sinc}(2B_0 t) \frac{\cos(2\pi\alpha B_0 t)}{1 - 16\alpha^2 B_0^2 t^2} \tag{9}$$

where

$B_0$: bandwidth of a specific system
$\alpha$: rolloff factor

Therefore, $P(t)$ is expressed as the convolution of $PN(t)$ and $F(t)$:

$$P(t) = \int_{-\infty}^{\infty} PN(t-s)F(s)ds \tag{10}$$

The reasons to use the Eq. (10) not the raised cosine pulse in [15] are (1) the simulation condition becomes the same as measurement; (2) the effect of the dynamic range is kept.

The delay profile that is obtained by sampling is therefore derived as follows:

$$\underline{h}(iT_s) = \sum_{l=1}^{L} A_l e^{j\psi_l} P(iT_s - \tau_l) \tag{11}$$

where $T_s$ is the chip or symbol duration. By introducing a parameter $\underline{A}_l$ as:

$$\underline{A}_l = A_l P(iT_s - \tau_l) \tag{12}$$

Equation (11) is rewritten as

$$\underline{h}(iT_s) = \sum_{l=1}^{L} \underline{A}_l e^{j\psi_l} \tag{13}$$

Equation (13) is then a similar formulation to the random phase approach proposed in [9] and [10].

The purpose of applying RPA here is to estimate the statistics of delay profiles without a full sampling process inside a small local area. If the receiving points inside this area are considered, the amplitude of an incident ray at different points is almost unchanged. Only

the phase of this ray is rotated due to the displacement. Within the unresolvable time period of a delay profile, these phase-rotations of different rays cause the local fading fluctuation of the delay profile. In order to address these effects, RPA is extend here. The total number of arrival rays and the amplitude of each ray are assumed to be unvaried during this small area. If the phase $\psi_i$ is assumed to be random, the cumulative probability function at each sampling instant is derived analytically. The value corresponding to 50% cumulative probability is selected to be a median value and the interval corresponding to the cumulative probabilities from 5% to 95% is selected to be a confidence interval. This 90% confidence interval can be considered as a fading deviation. The statistical median delay profile and the deviation of fading fluctuations are therefore calculated analytically.

### 4.2 Characterization of an Azimuth-Delay Profile

In micro- and pico-cellular environments, the elevation angles of received signals may not vary dramatically. An azimuth-delay profile therefore captures almost all the spatio-temporal characteristics of wireless channels. It is noted that several arrival rays may have the same incoming azimuth angles because incident rays at one scattering point may come from different points due to complicated reflection/diffraction phenomena. Accordingly, suppose that there are $Q$ ray groups (each group with the same azimuth degree) and $K_q$ rays in the $q$-th group, the band-limited spatio-temporal channel response (azimuth-delay profile) is then expressed as:

$$\underline{h}(\phi,\tau)=\sum_{q=1}^{Q}\sum_{k=1}^{K_q} A_{qk}e^{j\psi_{qk}}\delta(\phi-\phi_q)P(\tau-\tau_{qk}) \quad (14)$$

where $\phi$ represents the azimuth angle with respect to the beam direction. A 2-dimensional rectangular array antenna system is assumed in the simulation. Assuming the conventional beamformer and an omni-directional radiation pattern of each antenna element, the directivity pattern of the array antenna $D(\phi)$ is expressed as

$$D(\phi)=\sum_{m=1}^{M}\sum_{n=1}^{N}\exp(jk_0md\cos\phi)\exp(jk_0nd\sin\phi) \quad (15)$$

where $d$ represents the separation distance between elements. $m$ and $n$ represent the number of array element in $x$ and $y$ directions. $M$ and $N$ are the total number of array elements in $x$ and $y$ directions, respectively.

The band- and beamwidth-limited azimuth-delay profile is then obtained by:

$$\underline{\underline{h}}(\phi,\tau) = \int_0^{2\pi} \underline{h}(\psi,\tau)D(\phi-\psi)d\psi \quad (16)$$

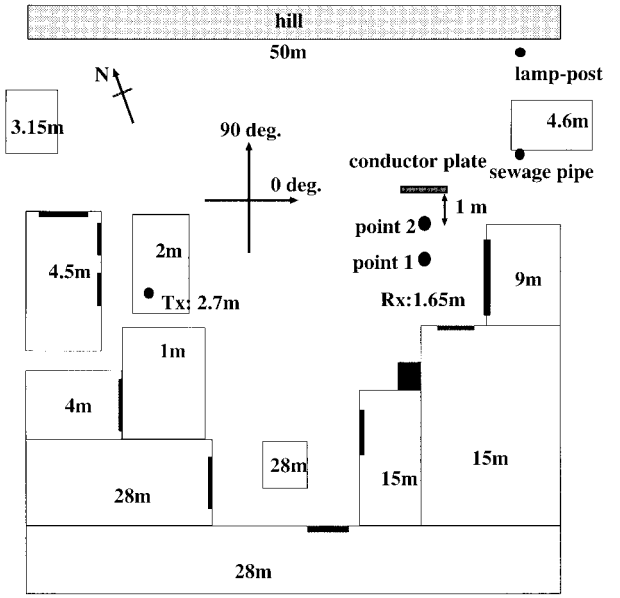


**Fig. 2** A pico-cell environment in YRP.

**Table 1** Electrical parameters used in ray-tracing.

| | Permittivity $\epsilon_r$ | Conductivity $\sigma$ [S/m] |
|---|---|---|
| building wall | 5.5 | 0.023 |
| ground plane | 15.0 | 0.005 |
| metal | - | $\infty$ |
| hill | 3.5 | 0.01 |

$$= \sum_{q=1}^{Q}\sum_{k=1}^{K_q} A_{qk}e^{j\psi_{qk}} \cdot D(\phi-\phi_q)P(\tau-\tau_{qk}) \quad (17)$$

## 5. Verification

Since future wideband wireless systems, such as Multimedia Mobile Access Communications Systems (MMAC) [16], are supposed to work at microwave bands (above 5 GHz), a pico-cell or a quasi-micro-cell environment served by these systems can be expected. A field measurement was carried out in Yokosuka Research Park (YRP). The measuring environment is a outdoor pico-cell environment (around $60\times60$ square meters), as shown in Fig. 2. The environment is complex with mixed heights of buildings and a nearby hill. A metal pillar and doors are indicated by a square black box and thin black boxes. The heights of a car, buildings and antennas are also shown in the figure. The electrical parameters used for ray-tracing calculation are shown in Table 1 [17]. The other simulation parameters are listed in Table 2.

In this measurement, a delay profile measurement system utilizing PN-sequence [18] is used. An 8.45 GHz spread-spectrum signal (10 W) with the chip

**Table 2** Simulation parameters used in ray-tracing.

| | |
|---|---|
| Frequency [GHz] | 8.45 |
| Tx antenna height [m] | 2.7 |
| Rx antenna height [m] | 1.65 |
| Reflection no. | 6 |
| Diffraction no. | 1 |
| PN-sequence stage | 11 |
| Chip duration [ns] | 20 |
| Bandwidth [MHz] | 100 |
| Rolloff factor | 0 |
| Tx and Rx Antennas | vertically polarized half-wave length dipole |

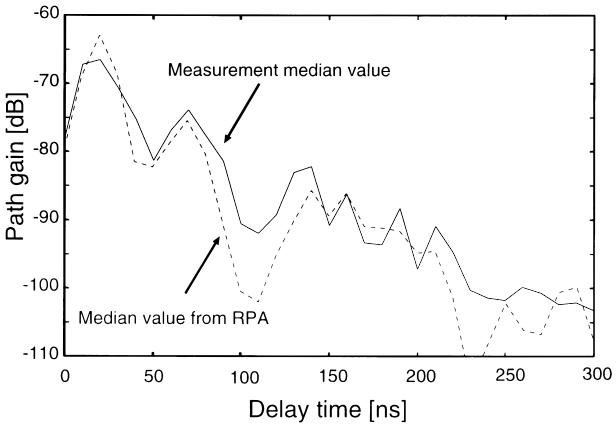


**Fig. 3** Comparison of the median delay profiles at point 1.

rate of 50 Mchips/s was transmitted. A high resolution (20 ns) was achieved. A PN sequence with a length of 2047 chips is adopted in the measurement and hence the whole dynamic range is above 60 dB ($20 \log_{10} 2047 \doteq 66$ dB). The whole bandwidth of this system is 100 MHz. A synthetic array approach is used here. It means that the receiving antenna is moved at $8 \times 8$ grid points with a $0.5\,\lambda$ separation distance between grids, to simulate a 2-dimensional array antenna with 64 elements. Measurements were done at two different receiving points. Since the scattering effects of a small hill near the receiving point can not be neglected, it is modeled as a tall rectangular obstacle. The effects of metal doors and pillars are also considered in the ray-tracing process. A conductor plate shown in the graph is used for the simulation of local scattering waves at point 2. This plate is supposed not to affect the arrival waves at two receiving points.

### 5.1 Verification of Delay Profiles

At each measurement point, the delay profiles corresponding to 5%, 50% and 95% cumulative probabilities are extracted from all 64 delay profiles. Figure 3 compares the median delay profile from ray tracing with measurement at point 1. A very good agreement is observed from the graph.

Next, in order to demonstrate the fading deviation predicted from RPA is trustworthy, Figs. 4, 5, 6, and 7 show the comparison of the fading deviation with measurement at point 1 when the measured delay profiles

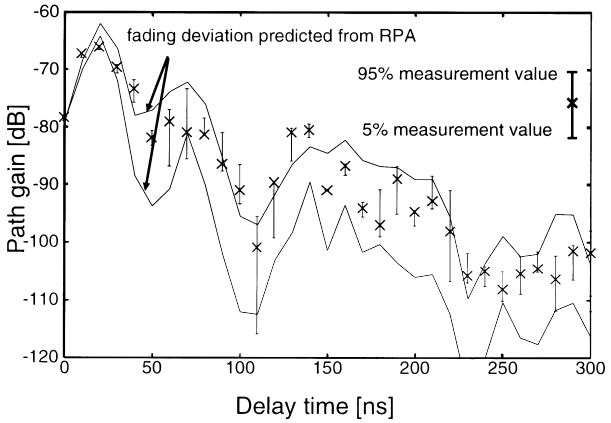


**Fig. 4** Illustration of the measured delay profiles taken from $1\,\lambda$ area size confined within the fading deviation predicted from RPA at point 1.

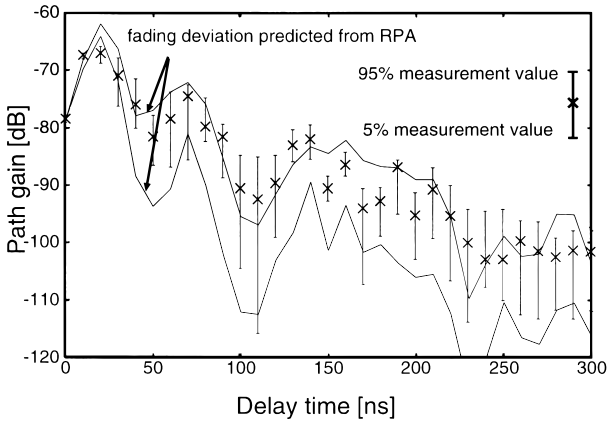


**Fig. 5** Illustration of the measured delay profiles taken from $2\,\lambda$ area size confined within the fading deviation predicted from RPA at point 1.

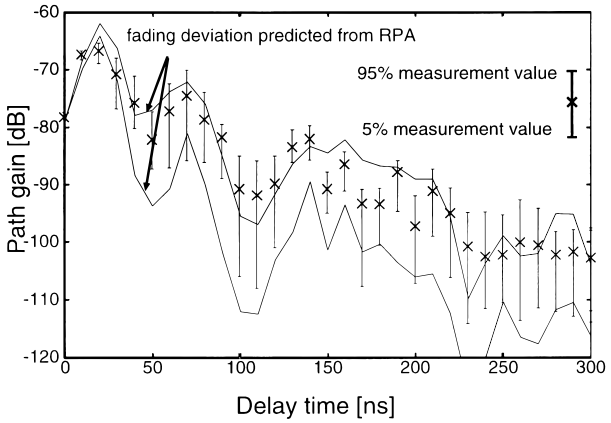


**Fig. 6** Illustration of the measured delay profiles taken from $3\,\lambda$ area size confined within the fading deviation predicted from RPA at point 1.

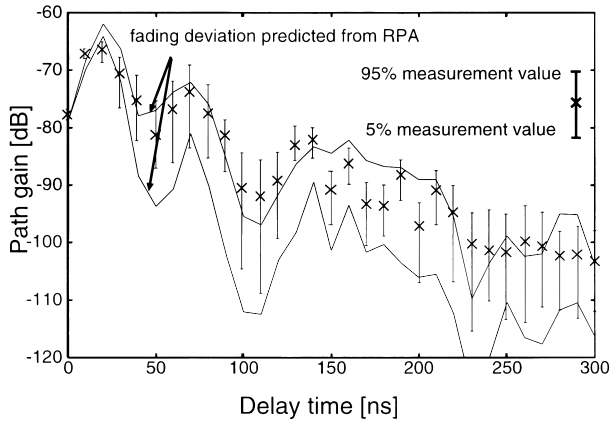


**Fig. 7** Illustration of the measured delay profiles taken from $4\,\lambda$ area size confined within the fading deviation predicted from RPA at point 1.

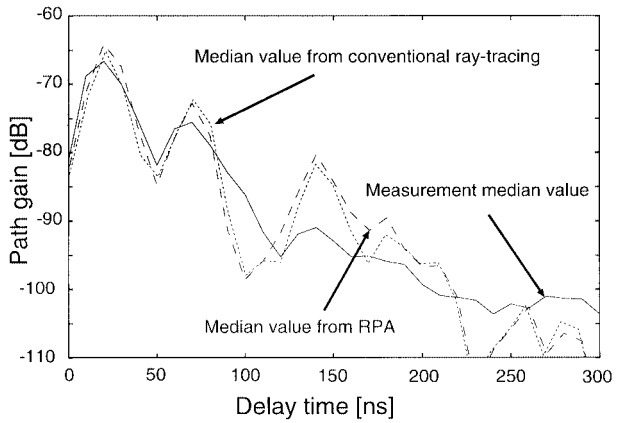


**Fig. 8** Comparison of the median delay profiles at point 2.

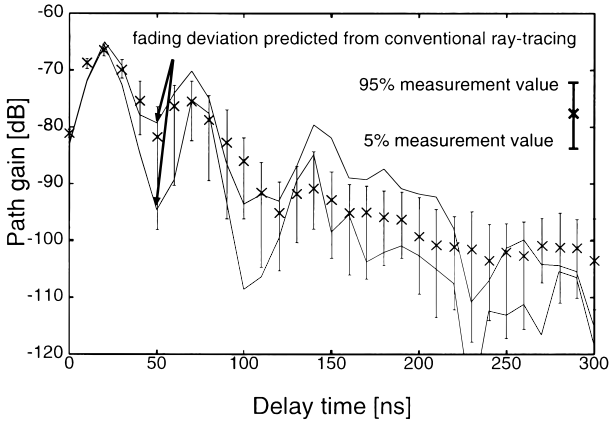


**Fig. 9** Illustration of the fading deviation extracted from conventional ray-tracing at point 2.

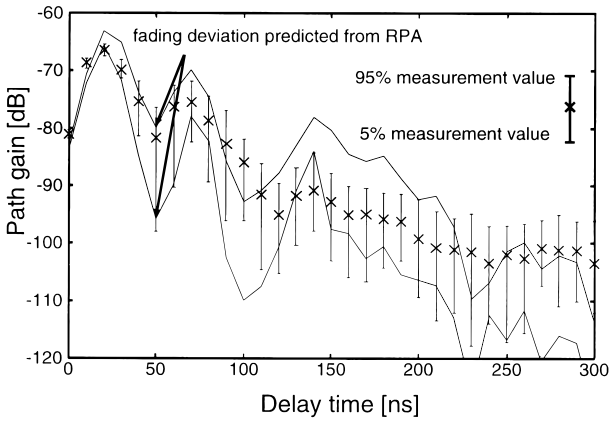


**Fig. 10** Illustration of the fading deviation predicted from RPA at point 2.

were taken from the area of different sizes. It is observed that the fluctuation range of measured delay profiles tend to increase when the size of area is increased. Overall, the measured delay profiles of 5% and 95% cumulative probabilities are all almost confined within the predicted fading deviation wherever the area size is increased from $1\,\lambda$ to $4\,\lambda$. These results prove that the RPA can predict an accurate fading fluctuation range of delay profiles within a small area ($8\ \text{grid} \times 0.5\,\lambda = 4\,\lambda$ in this case). Overall, both the median value and the range of fading fluctuations can be predicted by the RPA. It is then proved that the approach described in Sect. 4.1 is applicable in the real measurement.

At point 2, a high level of agreement is also observed in the comparison of the median delay profiles in Fig. 8. A peak at around 140 ns is somewhat overestimated by ray tracing. That may be caused by inaccurate modeling in electrical parameters of some buildings. Alternatively, a conventional ray-tracing process by spatially sampling at all 64 locations is also carried out at point 2. The median value and the fading deviation extracted from 64 delay profiles predicted from ray-tracing are illustrated in Fig. 8 and Fig. 9 respectively. Observed from Figs. 8, 9 and 10, there is very little difference between the results of the RPA and the conventional ray-tracing process. Since only one impulse response is necessary to derive the distribution by using RPA, the improved efficiency is $N$ times more than the conventional ray-tracing process. Here $N$ represents the number of necessary sampling points used by the conventional ray-tracing process. Thus, compared with the conventional process, the RPA is not only efficient but also very accurate without sacrificing the same accuracy as the conventional process has.

### 5.2 Verification of Azimuth-Delay Profiles

The measuring system and the transmitter and receiver settings are the same as those used in the measurement of delay profiles. The receiving antenna is moved at $8 \times 8$ grid points with a $0.5\,\lambda$ separation distance of grids. A $8 \times 8$ 2-dimensional array antenna system is therefore simulated. An azimuth-delay profile (beamforming pattern) of this antenna system is calculated and compared with the corresponding ray-tracing re-

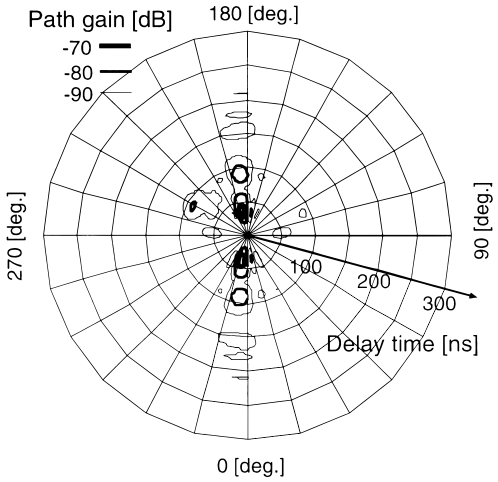


**Fig. 11** An contour plot of the measured azimuth-delay profile (point 1).

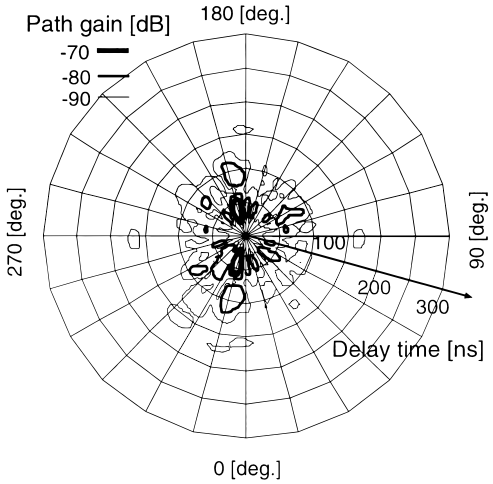


**Fig. 13** An contour plot of the measured azimuth-delay profile (point 2).

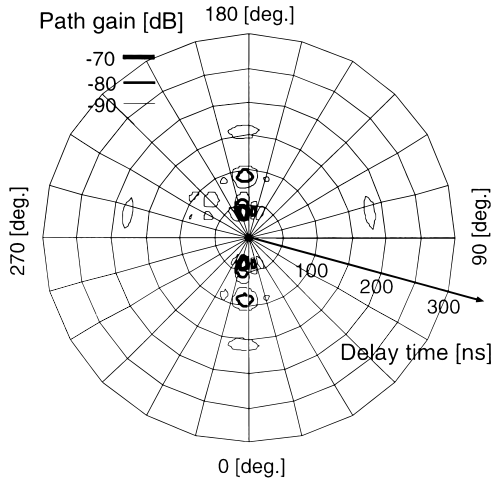


**Fig. 12** An contour plot of the azimuth-delay profile from ray tracing (point 1).

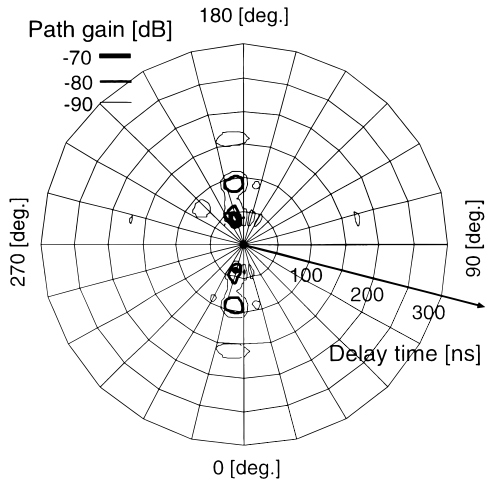


**Fig. 14** An contour plot of the azimuth-delay profile from ray tracing (point 2).

sults. The ray-tracing results are also transformed into the azimuth-delay profiles according to Sect. 4.2.

Figure 11 depicts the contour plot of the measured azimuth-delay profile at point 1. Figure 12 shows contour plot of the azimuth-delay profile transformed from CIR obtained by ray tracing. A high level of agreement is observed at the direct wave (190 degrees) and some scattering waves (240 and 350 degrees). Especially, the first, second and third arrival waves at 190 degrees and 350 degrees due to the multiple reflection between the wall and the car are all in good agreement. Some peaks at 100 and 260 degrees in the ray-tracing result are overestimated. The rough modeling of a hill with a rectangular stub may be the reason for that overestimated wave at 100 degrees.

Figures 13 and 14 show the contour plot of the azimuth-delay profiles at point 2. The good agreement is observed at the direct wave (200 degrees) and some scattering waves (around 225 degrees and 345 degrees). The first, second, third arrival waves at 200 degrees and 345 degrees are in good agreement and some waves from 10 degrees and 170 degrees are somewhat estimated, though the arrival angles have a little difference. However, the floor level of the measurement result seems to be quite high in spite of the dynamic range was the same as that at point 1. They almost have the the similar arrival time as the direct waves. The local scattering nearby the receiving antenna is the probable reason. To simulate this phenomenon, a rectangular conductor plate nearby the receiving location is assumed, which can be seen in Fig. 2. This plate is supposed not to affect other arrival waves but to introduce two diffraction waves along 40 degrees and 120 degrees. These waves can not be thought as the far-field plane waves. Different from the phase-rotation $(\boldsymbol{k}_i \cdot \boldsymbol{d}_m)$ in Eq. (5), the $\boldsymbol{k}_i$ is now different at every element and the phase-rotation become $\boldsymbol{k}_{im} \cdot \boldsymbol{d}_m$ now. This may cause the high measurement floor when using the beam-forming ap-

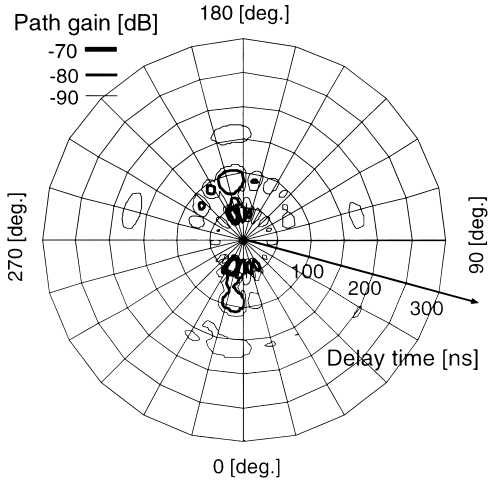


**Fig. 15** An contour plot of the azimuth-delay profile from ray tracing added with local scattered waves (point 2).

proach. Figure 15 show the azimuth-delay profile after adding these local scattering waves in the ray-tracing result. From the graph, the floors are obviously raised in Fig. 15. This result proves that local scattering is the probable reason.

Overall, a good accuracy of the transformed azimuth-delay profile from ray tracing is observed in these comparisons. From the comparisons in Sects. 5.1 and 5.2, the overall simulation process, i.e., ray tracing, a random phase approach, band- and beamwidth-limitation, proved to be accurate.

## 6. Conclusion

This paper investigates a spatio-temporal channel modeling approach based on ray tracing. A spatio-temporal channel model is proposed and the spatio-temporal CIR is obtained from a 2D-3D hybrid ray-tracing method. The focuses of this paper are to extend the RPA for predicting local fading fluctuation of delay profiles and to explore the applicability of deterministic modeling in predicting spatio-temporal channel characteristics. The statistics of delay profiles and the azimuth-delay profiles predicted from ray tracing are verified with a pico-cell measurement. The following observations are obtained:

1. A range of fading fluctuations as well as median values can be correctly predicted by using the RPA.
2. To estimate the statistics of delay profiles, the RPA is not only much more efficient than the conventional ray-tracing process, but also very accurate.
3. A very good agreement is observed between the measured azimuth-delay profiles and the results transformed from ray-tracing. That proves that deterministic modeling under specific system conditions is applicable.
4. Local scattering has to be carefully avoided in the measurement with using a synthetic aperture. That raises the measurement floors.

Finally, these verifications provide a solid ground of applying ray-tracing approaches in analysis of the performance of specific systems in real environments.

## Acknowledgement

The authors would like to thank K. Sakaguchi, J. Fu, and K. Shimano of Tokyo Institute of Technology, H. Masui, H. Shimizu, M. Ishii and K. Sakawa of YRP Key Tech Labs for their cooperation and help in the experiments. The authors would also like to thank Dr. T. Taga of NTT DoCoMo Co., for his many helpful discussions and suggestions. This work is partly supported by the Scientific Grant in Aid from Japanese Ministry of Education.

### References

[1] R.B. Ertel, P. Cardieri, K.W. Sowerby, T.S. Rappaport, and J.H. Reed, "Overview of spatial channel models for antenna array communication systems," IEEE Personal Commun., vol.5, no.2, pp.10–22, Feb. 1998.
[2] B.H. Fleury and P.E. Leuthold, "Radiowave propagation in mobile communications: An overview of European research," IEEE Commun. Mag., vol.34, no.2, pp.70–81, Feb. 1996.
[3] J.C. Liberti and T.S. Rappaport, "A geometrically based model for line-of-sight multipath radio channels," IEEE Veh. Technol. Conf., pp.844–848, April 1996.
[4] M. Lu, T. Lo, and J. Litva, "A physical spatio-temporal model of multipath propagation channels," IEEE Veh. Technol. Conf., pp.180–184, 1997.
[5] R.A. Valenzuela, "A ray tracing approach for predicting indoor wireless transmission," IEEE Veh. Technol. Conf., pp.214–218, 1993.
[6] S.Y. Seidel and T.S. Rappaport, "Site-specific propagation prediction for wireless in-building personal communication system design," IEEE Trans., Veh. Technol., vol.43, no.4, pp.879–891 Nov. 1994.
[7] T. Furuno and T. Taga, "Identification of propagation path from low antenna height base station in urban area," IEICE Trans., vol.J83-B, no.1, pp.71–80, Jan. 2000.
[8] H. Zhu, J. Takada, and K. Araki, "Ray-tracing-based spatio-temporal channel modeling for multimedia mobile access communication systems (MMAC)," 10th International Symposium on Personal, Indoor and Mobile Radio Communications, pp.116–120, Osaka, Sept. 1999.
[9] S. Takahashi and Y. Yamada, "Propagation-loss prediction using ray tracing with a random-phase technique," IEICE Trans. Fundamentals, vol.E81-A, no.7, pp.1445–1451, July 1998.
[10] H. Zhu, J. Takada, K. Araki, and T. Kobayashi, "Verification of a 2D-3D hybrid ray-tracing method for spatio-temporal channel modeling," Radio Science, vol.36, no.1, pp.53–66, Jan./Feb. 2001.
[11] J.C. Liberti and T.S. Rappaport, Smart Antennas for Wireless Communications: IS-95 and 3rd Generation CDMA Applications, Prentice Hall, 1999.
[12] J.D. Foley, A. van Dam, S.K. Feiner, and J.F. Hugheds.,

Computer Graphics Principles and Practice, Addison-Wesley, 1997.
[13] O. Landron, M.J. Feuerstein, and T.S. Rappaport, "A comparison of theoretical and empirical reflection coefficients for typical exterior wall surfaces in a mobile radio environment," IEEE Trans. Antennas & Propag., vol.44, no.3, pp.341–351, March 1996.
[14] R.J. Luebbers, "Finite conductivity uniform GTD versus knife edge diffraction in prediction of propagation path loss," IEEE Trans. Antennas & Propag., vol.AP-32, no.1, pp.70–76, Jan. 1984.
[15] H. Zhu, J. Takada, K. Araki, H. Masui, M. Ishii, K. Sakawa, H. Shimizu, and T. Kobayashi, "A ray-tracing-based spatio-temporal channel model and its validation," Proc. 2000 IEICE general conference, SB-1-6, pp.713–714, Hiroshima, March 2000.
[16] URL: http://www.arib.or.jp/mmac/e/
[17] CCIR Rec. 527-2, "Electrical characteristics of the surface of the Earth," ITU, Geneva, 1991.
[18] H. Masui, K. Takahashi, S. Takahashi, K. Kage, and T. Kobayashi, "Delay profile measurement system for microwave broadband transmission and analysis of delay characteristics in an urban environment," IEICE Trans. Electron., vol.E82-C, no.7, pp.1287–1292, July 1999.

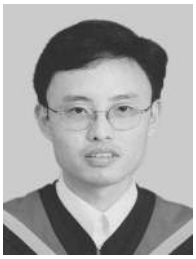

**Houtao Zhu** was born in Shanghai, China, in l968. He received his B.E. from Shanghai Jiao Tong University, Shanghai, China, in 1991 and received his M.E. from Asian Institute of Technology, Bangkok, Thailand, in 1996. Currently he is studying towards the D.E. degree in Tokyo Institute of Technology, Tokyo, Japan. His main research interests are propagation prediction modeling, wireless channel modeling, smart antennas and wireless communications. He is a student member of IEEE.

**Jun-ichi Takada** was born in Tokyo in l964. He received B.E., M.E. and D.E. Degrees from Tokyo Institute of Technology, in 1987, 1989 and 1992, respectively. In 1992–1994. he was a research associate in Chiba University. Japan. From 1994 he is an associate professor at Tokyo Institute of Technology. He received the Excellent Paper Award and Young Engineer Award from IEICE Japan in 1993 and 1994, respectively. His current research interests are array signal processing, mobile communication and numerical simulation of waves. He is a member of ITEJ, IEEE, SIAM, AGU and ACES.

**Kiyomichi Araki** was born in Nagasaki on January 7, 1949. He received the B.S. degree in electrical engineering from Saitama University, in 1971, and the M.S. and Ph.D. degrees in physical electronics both from Tokyo Institute of Technology, in 1973 and 1978, respectively. In 1973–1975, and 1978–1985, he was a Research Associate at Tokyo Institute of Technology, and in 1985–1995 he was an Associate Professor at Saitama University. In 1979–1980 and 1993–1994 he was a visiting research scholar at University of Texas, Austin and University or Illinois, Urbana, respectively. He is currently a Professor at Tokyo Institute of Technology. Dr. Araki is a member of IEEE and Information Society of Japan. His research interests are information security, coding theory, communication theory, circuit theory, electromagnetic theory, microwave circuits etc.

**Takehiko Kobayashi** received the B.S., M.S., and Ph.D. degrees in electronic engineering from the University of Tokyo, Tokyo, Japan, in 1978 and 1980 and 1983. He joined the Electrical Communication Laboratory of NTT in 1983 and was engaged in research in communication antennas, engineering aspects of bioelectromagnetics, and EMC. He was a guest scientist at the National Bureau of Standards (now NIST) of the US Department of Commerce, Boulder, Colorado from 1986 to 1987. From 1997 to 1998 he was a senior manager/special advisor to Multimedia Development Corporation, Malaysia to plan and coordinate Malaysia's Multimedia Super Corridor project. He joined YRP Key Tech Labs in 1998 as Head of the Communication Systems Department. He is a member of IEEE.